RESEARCH PAPER

Smartphone coupled with paper-based chemical sensor for on-site determination of iron(III) in environmental and biological samples

Kamlesh Shrivas[1] · Monisha[1] · Tushar Kant[1] · Indrapal Karbhal[1] · Ramsingh Kurrey[1] · Bhuneshwari Sahu[1] · Deepak Sinha[2] · Goutam Kumar Patra[3] · Manas Kanti Deb[1] · Shamsh Pervez[1]

Abstract

We report a smartphone–paper-based sensor impregnated with cetyltrimethylammonium bromide modified silver nanoparticles (AgNPs/CTAB) for determination of Fe^{3+} in water and blood plasma samples. The methodology for determination of Fe^{3+} is based on the change in signal intensity of AgNPs/CTAB fabricated on a paper substrate after the deposition of analyte, using a smartphone followed by processing with ImageJ software. The mechanism of sensing for detection and determination of Fe^{3+} is based on the discoloration of AgNPs which impregnated the paper substrate. The discoloration is attributed to the electron transfer reaction taking place on the surface of NPs in the presence of CTAB. Fe^{3+} was determined when the paper was impregnated with 1 mM AgNPs for 5 min of reaction time and the substrate was kept under acidic conditions. The linear range for determination of total iron in terms of Fe^{3+} was 50–900 $\mu g \, L^{-1}$ with a limit of determination (LOD) of 20 $\mu g \, L^{-1}$ and coefficient of variation (CV) of 3.2%. The good relative recovery of 91.3–95.0% and interference studies showed the selectivity of the method for determination of total iron in water and blood plasma samples. Smartphone–paper-based sensors have advantages of simplicity, rapidity, user-friendliness, low cost, and miniaturization of the method for on-site determination of total iron compared to methods that require sophisticated analytical instruments.

Keywords Smartphone · Paper sensor · AgNPs/CTAB · ImageJ software · Fe^{3+} · Water and blood samples

Introduction

Iron (Fe) is the most abundant transition metal in the earth's crust, water, and food and vegetable samples. Iron naturally occurs in the forms of Fe^{2+} and Fe^{3+} in water and food samples. The threshold limit value (TLV) of iron (Fe^{2+} and Fe^{3+}) recommended by the World Health Organization (WHO) in drinking water is 0.3 $mg \, L^{-1}$. Iron is an essential trace element that plays several roles in biochemical and intracellular processes like electron transport, DNA synthesis, and oxygen transport through hemoglobin [1–4]. Excess intake of iron through food and water may induce the formation of active oxygen species in the body which results in oxidation and damage of proteins, nucleic acids, and lipids. This biochemical process results in conditions like carcinoma, Alzheimer's, Parkinson's, and Huntington's diseases in human beings; however, deficiency of iron may result in anemia, fatigue, and impaired immunity [5–7]. Hence, determination of iron in water and plasma samples is of great interest to ensure public health.

Several analytical methods including spectrophotometry [8–10], voltammetry [11, 12], atomic absorption spectroscopy (AAS) [13, 14], inductive coupled plasma–atomic emission spectroscopy (ICP-AES) [15], and X-ray fluorescence (XRF) [16] have been reported for determination of iron in environmental, vegetable, and biological samples. Most of these techniques such as voltammetry, AAS, ICP-AES, and XRF involve time-consuming and tedious sample preparation procedures before the

✉ Kamlesh Shrivas
kshrivas@gmail.com

1 School of Studies in Chemistry, Pt. Ravishanakar Shukla University, Raipur, CG 492010, India

2 Department of Chemistry, Government Nagarjuna Post Graduate College of Science, Raipur, CG 492010, India

3 Department of Chemistry, Guru Ghasidas Vishwavidyalaya, Koni, Bilaspur, CG 495009, India

instrumental analysis; however, these techniques are sensitive. Spectrophotometry is simple and rapid for determination of iron in a variety of samples through the formation of colored complexes with chromophoric reagents and analyte present in the sample. In addition, this technique can be applied at the sample source for determination of iron owing to the small size of the instrument. Woods and Mellon reported the determination of iron via formation of a red-colored complex with thiocyanate ions in the presence of hydrochloric acid. Spectrophotometric methods are still in use for determination of iron in various samples owing to their facile procedures, but the sensitivity of the methods is low [8]. Other chromophoric reagents such as Tiron [10], leucoxylene cyanol [17], 1,2-dihydroxy-3,4-diketocyclobutene [18], and morin [19] have been reported for determination of iron in various types of samples. The drawback of spectrophotometric methods is the use of chromophoric reagents that are sometimes not selective for determination of the target analyte. Therefore, an alternative method is needed for determination of iron in water samples at the sample source and it should be free from the requirement of chromophoric reagents.

Recently, silver (Ag), gold (Au), and copper (Cu) metal nanoparticles (NPs) have been widely used as colorimetric sensors for determination of different types of chemical substances [20, 21]. In addition, composite nanomaterials are also exploited for efficient catalytic activity of pollutants from environmental samples [22, 23]. In colorimetric determination, the changes in color transition of AgNPs from yellow to violet, and AuNPs from pink to blue, and CuNPs from red to yellow followed by the red shift of localized surface plasmon resonance (LSPR) of these NPs in the visible region are exploited as chemical sensors for determination of metal ions [24], pesticides [25–27], bisphenol A [28], cationic surfactants [29], drugs [30, 31], and thymine [32] in environmental, food, biological, and pharmaceutical samples. The drawbacks of these NP-based colorimetric sensors are use of large volume (ca. 5 mL) of NP solution and use of expensive spectrophotometric (colorimetric) instruments assisted by a computer control unit. Thus, we developed a simple method in which a smartphone is used for determination total iron in water samples and that avoids the use of large amounts of NP solution and a spectrophotometric instrument.

More recently, paper-based analytical devices (PADs) have drawn wide interest owing to their simplicity, portability, rapidity, cost-effectiveness, and low consumption of reagents and sample. PADs are based on development of color after chemical reaction between the analyte and reagent fabricated on the paper substrate. This color change is either measured by digital camera, smartphone, or the unaided human eye [33, 34]. Ratnarathorn et al. developed PADs for quantitative determination of copper using homocysteine and dithiothreitol modified AgNPs based on the formation of coordination complex between the analyte and capping agent that caused the color change of NPs on the surface of the paper substrate [35]. Apilux et al. demonstrated the use of a paper sensor for determination of Hg^{2+} in real water samples based on the color change of silver nanoplate after the introduction of analyte on the test zone of the paper substrate [36]. Chen et al. illustrated the use of low-cost PADs for determination of the freshness of vegetables which depends on the color change of dye deposited on the paper substrate after the release of volatile organic compounds from food samples [37]. On the basis of the use of PADs for analysis of variety of chemical substances in biological, environmental, and vegetable samples, we tried to integrate the exploitation of a smartphone–paper-based sensor for determination of iron at the sample source.

In the present work, a smartphone–paper-based sensor impregnated with AgNPs/CTAB has been developed for easy determination of ferric iron from water and blood plasma samples. Here, smartphone is used to record an image of the paper substrate after the deposition of analyte followed by processing with ImageJ software for quantitative determination of Fe^{3+}. The analytical factors such stabilizing agent, concentration of NPs, pH, and reaction time are optimized for determination of analyte from sample solution. The sensing mechanism for determination of Fe^{3+} using the smartphone coupled with paper-based sensor has been illustrated and validated using transmission electron microscopy (TEM), UV–visible (UV–Vis) spectrophotometry, and Fourier transforms infrared (FTIR) spectroscopy.

Experimental section

Reagents and solution preparations

All the chemicals were used of analytical grade reagent. Silver nitrate ($AgNO_3$), sodium borohydride ($NaBH_4$), 1,10-phenanothroline, hydrochloric acid (HCl), sodium hydroxide (NaOH), and metal salts were obtained from Hi-media (Mumbai, India). Cetyltrimethylammonium bromide (CTAB), cetyltrimethylammonium chloride (CPC), trisodium citrate, and ferric ammonium sulfate were purchased from Sigma Aldrich (MA, US). Stock standard solutions of Fe^{3+} and other metal ions (100 μg mL^{-1}) were prepared by dissolving an appropriate amount of the respective chemical substance in separate glass vials in distilled water (DW). Filter paper no. 1 was purchased from Avantor Performance Materials Pvt. Ltd. (Thane, India). The different pH of solutions was achieved using 0.1 M HCl and 0.1 M NaOH solutions. The working standard solution of each metal ion was prepared by the diluting the stock standard solution of metal ions.

Sampling of water and blood plasma for determination of Fe^{3+}

Samples of surface water ($n = 4$), groundwater ($n = 3$), and industrial wastewater ($n = 1$) were collected from different locations of Raipur, Chhattisgarh during the month of March–April, 2019 using polyethylene bottles. All the water samples were acidified with 0.01 M HCl at the sampling site to avoid the precipitation of Fe^{3+} during the exposure to ambient environment including sunlight [38]. The samples were stored in a refrigerator at 4 °C and filtered using Whatman filter paper no. 42 prior to chemical analysis.

The blood plasma samples ($n = 2$) were collected in polyethylene bottle from healthy volunteers with the help of trained personnel of a local hospital of Raipur city. Consent was obtained from the concerned person for the performance of the experiment. All the experiments were performed in compliance with the relevant laws and institutional guidelines as well as the approval from the research committee of the university and hospital of Raipur city. A 1-mL aliquot of plasma sample was added into a beaker containing 7 mL DW and 5 mL of 2 N HCl [39] and the mixture was heated on a water bath for 3 min. The mixture was filtered with Whatman filter paper no. 42 and the filtrate was used for determination of Fe^{3+} using the smartphone–paper-based sensor.

Synthesis of bare, CTAB, citrate, and CPC-capped AgNPs

Bare, CTAB, CPC, and citrate-capped AgNPs were prepared by the reduction of $AgNO_3$ with $NaBH_4$ in the presence of the respective stabilizing agents [40]. The bare AgNPs were synthesized by the reduction of $AgNO_3$ using $NaBH_4$ as a reducing agent. For this, 10 mL of 1.0×10^{-3} M $AgNO_3$ was added into a 50-mL conical flask and kept in an ice bath for 10 min whilst constantly stirring followed by the introduction of 1 mL of 0.01 M $NaBH_4$ solution. Similarly, CTAB-capped AgNPs were synthesized in the presence of $NaBH_4$ as a reducing agent and CTAB as a capping agent. For this, 10 mL of 1.0×10^{-3} M $AgNO_3$ was added into a conical flask along with 1 mL of 0.03 M CTAB; the mixture was stirred for 20 min in an ice bath followed by addition of 1 mL of 0.01 M $NaBH_4$. After complete addition of $NaBH_4$, the mixture was further stirred for 20 min and a color change was observed from colorless to yellow, indicating the formation of CTAB-capped AgNPs. Consequently, CPC-capped AgNPs were prepared in the presence of CPC as a stabilizing agent. For this, 10 mL of 1.0×10^{-3} M $AgNO_3$ and 1 mL of 0.03 M CPC were added into a conical flask and the mixture was stirred for 20 min. After, 1 mL of 0.01 M $NaBH_4$ was added dropwise and the appearance of yellow color indicated the formation of CPC-capped AgNPs. Citrate-capped AgNPs were prepared by adding 10 mL of 1.0×10^{-3} M $AgNO_3$ and

1 mL of 0.03 M CPC into a conical flask and the mixture was stirred for 20 min. After, 1 mL of 0.01 M $NaBH_4$ was added dropwise and the appearance of yellow color indicated the formation of citrate-capped AgNPs. The concentration of bare, CTAB, CPC, and citrate-capped AgNPs used for fabrication of the paper-based device was 1.0 mM.

Preparation of paper-based sensor impregnated with AgNPs

Filter paper no. 1 was punched into 1.0-cm-diameter circular discs for preparation of the AgNPs-impregnated paper-based sensor. The circular discs were stacked on the paper which had a hydrophobic surface to prevent the spreading of solution from the test zones. Next, 50 μL of 1 mM AgNPs was deposited on each test zone of the paper disc and dried at room temperature. The impregnated paper with AgNPs was further used for determination of ferric irons from sample solutions.

Apparatus

An Evolution 300 UV–visible (UV–Vis) spectrophotometer (Thermo Scientific, USA) equipped with a quartz cell of path length 1 cm was used for measurement of the absorbance of AgNPs solutions. A Nicolet 10 FTIR spectrometer (Thermo Scientific, USA) was used for measurement of IR spectra of pure CTAB, AgNPs/CTAB, and solution mixture of AgNPs/CTAB with Fe^{3+}. A Tecnai F30 FEG TEM instrument was applied at an accelerating voltage of 300 kV for determination of the size and shape of AgNPs/CTAB in the presence and absence of analyte.

Determination of total iron in terms of Fe^{3+} using smartphone–paper-based sensor impregnated with AgNPs

Aliquots (50 μL) of Fe^{3+} standard solutions (50–900 μg L^{-1}) were deposited on test zones of the filter paper and dried at room temperature. The color of AgNPs changed from yellow to colorless depending on the amount of deposition of analyte. An image of the paper substrate was recorded using a smartphone followed by processing in ImageJ software to determine the color intensity versus the different concentrations of analyte. A calibration curve was prepared between different concentrations of Fe^{3+} and signal intensity obtained by the ImageJ software. Similarly, the total iron present in water was determined by depositing water/blood plasma samples (50 μL) on the paper substrate, adding 1.0×10^{-3} M $KMnO_4$ (10 μL) to oxidize the ferrous ions (Fe^{2+}) in the water samples to ferric ions (Fe^{3+}), and drying at room temperature. A smartphone was used to record the color and ImageJ software was used to calculate the color intensity after addition of sample solution. A 1.0-cm^2 sample size area was selected for

determination of signal intensity for different sets of experiments. The calibration curve was used for determination of total iron in terms of Fe^{3+} in samples. The processing of signal intensity of analyte on the paper substrate was done by considering the background signal processing and S/N ratios for negative control for accuracy of the method. Figure 1 shows a schematic diagram for determination of total iron using the smartphone–paper-based sensor.

Results and discussion

Assay for determination of Fe^{3+} using smartphone–paper-based sensor impregnated with AgNPs/CTAB

The screening of metals ions (Na^+, K^+, Al^{3+}, Mg^{2+}, Cr^{3+}, Ca^{2+}, Fe^{3+}, Ni^{2+}, Co^{2+}, Cu^{2+}, Zn^{2+}, Ba^{2+}, Cd^{2+}, As^{3+}, La^{3+}, Yb^{3+}, Pb^{2+}, Hg^{2+}, Tb^{3+}, and Gd^{3+}) was performed for selective determination by depositing 50 μL of different metal ions (1 μg mL^{-1}) on test zones of filter paper impregnated with AgNPs/CTAB. The results are shown in Fig. 2A. The discoloration of NPs was obtained only with Fe^{3+} and not with other metal ions deposited on the paper substrate. The deposition of different metal ions on the paper substrate exhibited the same color as the silver NPs showing that there might not be any interaction of these metal ions with NPs. However, the

discoloration was observed with Fe^{3+}, illustrating the interaction of analyte with AgNPs. Further, the color change with ferric iron not with other metal ions was verified by recording their images with a smartphone. The results are shown in Fig. 2B. The yellow colored bar diagram shows the color intensity of AgNPs before and after addition of different metal ions obtained by ImageJ software. Bars of same color intensity were found for all metal ions except the ferric iron which showed a decrease in signal intensity. In addition, the control experiment was performed to determine the variation of signal intensity after the deposition of AgNPs on several paper discs. The result is shown in Fig. S1 (see Electronic Supplementary Material, ESM). The SD value of 9.2 and CV value of 2.1% demonstrated that there is no significant change in the variation of signal intensity between different discs for analysis of Fe^{3+}. Thus, the results from ImageJ software confirmed the qualitative data for determination of ferric iron using the smartphone–paper-based sensor.

Next, the results obtained by ImageJ software were verified using colorimetric measurements by spiking different concentrations of metal ions (1 μg mL^{-1}) into a glass vial containing 1 mL of AgNPs/CTAB and the total volume of the solution was made up to 3 mL with DW. The results are shown in ESM Fig. S2a–u. The color change of AgNPs from yellow to colorless was observed only with Fe^{3+} ion (ESM Fig. S3h) and not with other metal ions (ESM Fig. S2b–g and i–u) which illustrated the selectivity for determination of target analyte
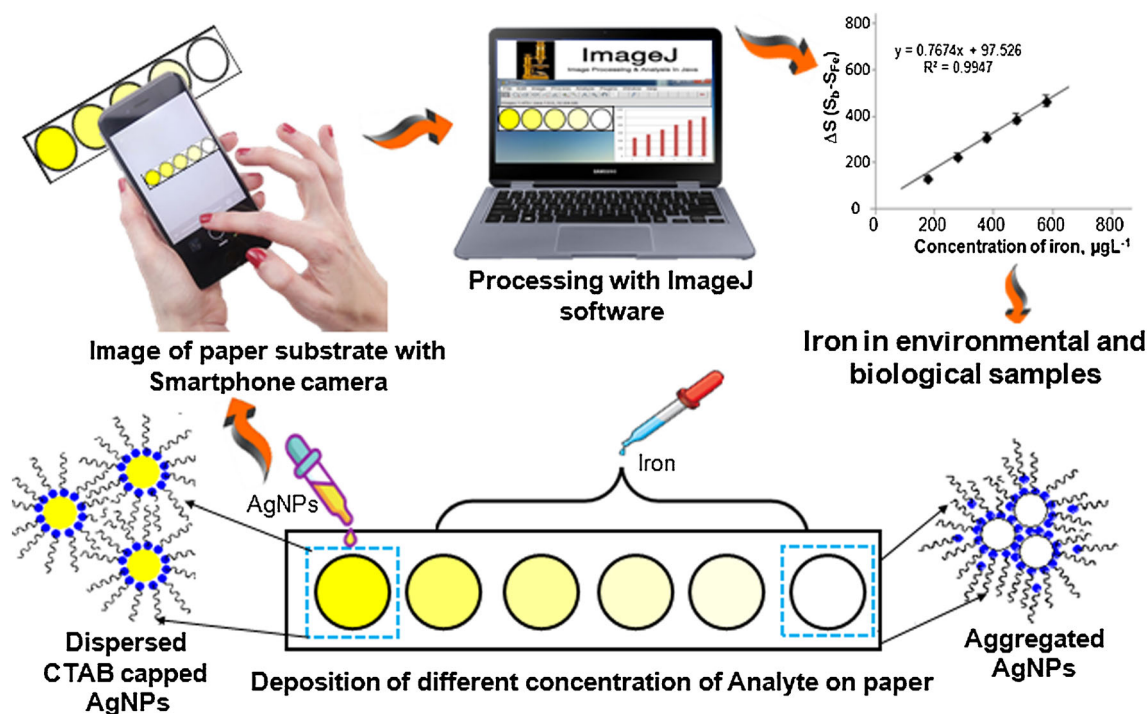
Fig. 1 Schematic diagram to demonstrate the use of smartphone–paper-based sensor followed by processing in ImageJ software to determine the calibration curve and total iron in unknown environmental water and biological samples

Fig. 2 **A** Test zone of filter paper with deposition of AgNPs/CTAB and different metal ions showing yellow color as the NPs and only AgNPs with Fe^{3+} showed the discoloration. **B** Color bar intensity of AgNPs/CTAB with different metal ions and similarly ferric iron showed the lowest signal intensity with NPs
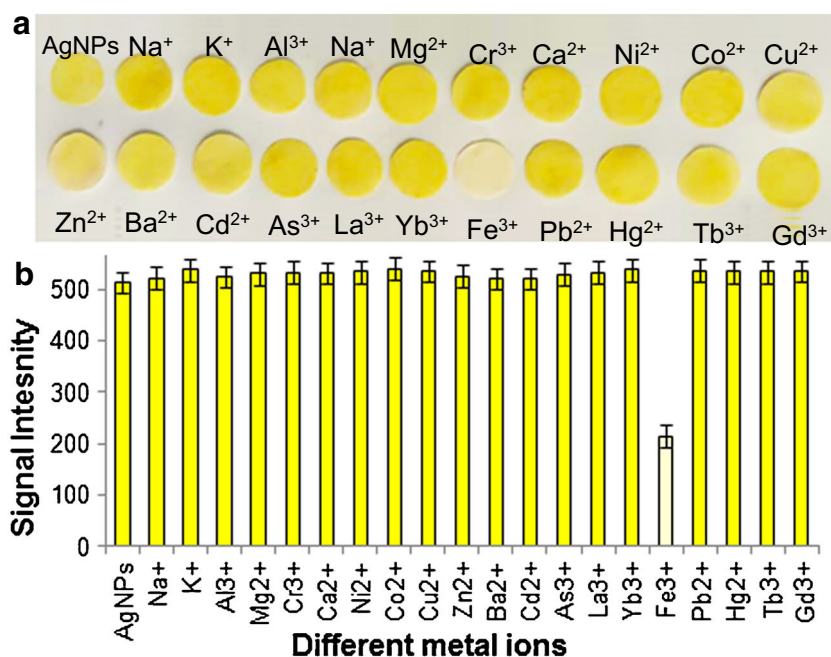
from sample solutions. Therefore, AgNPs capped with CTAB were exploited as a sensing probe for selective determination of target analyte from sample solution. The LSPR absorption peak (at 400 nm) obtained for different metals ions was similar to that for AgNPs/CTAB which demonstrated that there might be no interaction after the addition of metal ions into the NPs solution. The discoloration and hypochromic shift of the LSPR band were observed only with ferric iron. The color change of AgNPs from yellow to colorless is due to the interaction between Fe^{3+} with CTAB-capped AgNPs. Therefore, we tried to develop a novel smartphone–paper-based sensor for selective determination of ferric irons from sample solutions.

The role of stabilizing agent present on the surface of AgNPs was checked by analyzing Fe^{3+} with bare, CTAB, CPC, and citrate-capped AgNPs. Here, bare, CTAB, CPC, and citrate-capped AgNPs were placed separately on the paper substrate followed by the addition of Fe^{3+}. The deposition of ferric iron on the paper substrate impregnated with AgNPs/ CTAB showed the discoloration; and CPC, citrate, and bare NPs did not show any change after addition of analyte, as shown in ESM Fig. S3a–d. In addition, the color intensity of paper substrate impregnated with CTAB, CPC, citrate, and bare NPs was determined using ImageJ software and their respective bar diagrams are shown in ESM Fig. S3a–d. The same color intensity was acquired when the ferric iron was placed on the paper substrate impregnated with CPC, citrate, and bare AgNPs. The decrease in signal intensity was observed only with CTAB-capped AgNPs. These results demonstrated that the stabilization of AgNPs with CTAB is essential for interaction with ferric iron. Hence, the paper substrate

impregnated with CTAB-capped AgNPs was further exploited for determination of ferric irons from sample solutions.

The selectivity for determination of Fe^{3+} was done by analyzing Fe^{2+} with the paper-based sensor under the same experimental conditions. For this, CTAB-capped AgNPs were deposited on five test zones of the paper substrate followed by addition of (a) AgNPs, (b) AgNPs + Fe^{3+}, (c) AgNPs + Fe^{2+}, (d) AgNPs + Fe^{2+} + $KMnO_4$, and (e) AgNPs + $KMnO_4$ (Fig. 3). The introduction of Fe^{3+} on the paper substrate showed the color change from yellow to colorless (Fig. 3b). No color change was observed when Fe^{2+} was added onto the paper containing AgNPs/CTAB because Fe^{2+} may not interact with CTAB-capped NPs (Fig. 3c). However, the paper substrate containing Fe^{2+} followed by the addition of $KMnO_4$ exhibited the discoloration of NPs (Fig. 3d) because the $KMnO_4$ oxidized Fe^{2+} to Fe^{3+} and the latter interacted with CTAB. Further, the control blank experiment was performed by depositing AgNPs and $KMnO_4$ on the paper substrate without the introduction of analyte to check whether the addition of $KMnO_4$ affected the determination of iron (Fig. 3e). Thus, the paper-based sensor impregnated with AgNPs/CTAB was used for determination of total iron (Fe^{2+} and Fe^{3+}) present in water sample solutions.

Optimization of smartphone–paper-based sensor impregnated with AgNPs/CTAB for determination of Fe^{3+}

The pH of the paper-based sensor was optimized by placing the 50 μL of solutions of different pH (3.0, 5.0, 7.0, 9.0, and 11.0) on the paper substrate containing NPs and Fe^{3+}.

Fig. 3 Paper substrate containing **a** AgNPs, **b** AgNPs + Fe^{3+}, **c** AgNPs + Fe^{2+}, **d** AgNPs + Fe^{2+} + KMnO$_4$, and **e** AgNPs + KMnO$_4$ along with the respective bar diagram obtained with ImageJ software
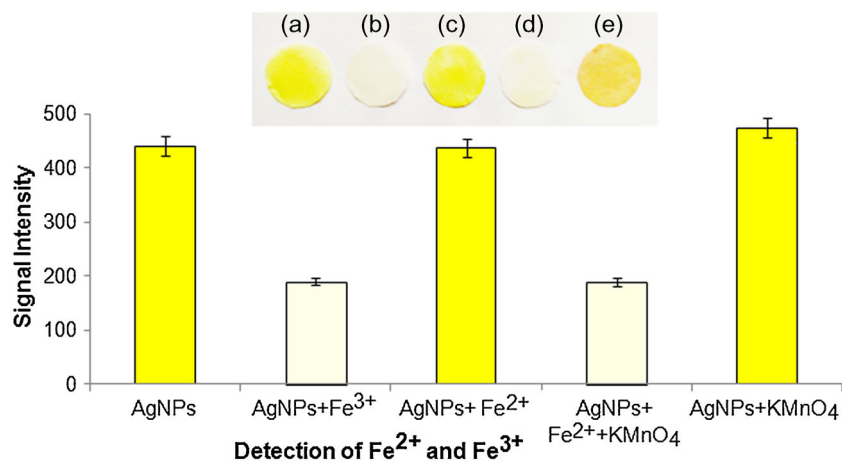
Discoloration of the spot and the maximum difference in signal intensity (ΔS) were found when the pH was between 3.0 and 5.0 (ESM Fig. S4A). Better results were obtained under acidic conditions because the chemical reaction is favored at this pH range [41]; however, when the pH of the paper substrate was varied from 7.0 to 11.0, no color change was obtained. This is due to the formation of ferric hydroxide complex in the pH range of 7.0–11.0 which reduces the concentration of freely available Fe^{3+} [42] and thus all the experiments were performed under acidic conditions. The reaction time was optimized by depositing the standard solution of ferric ions on the paper substrate and the maximum discoloration of AgNPs was monitored. The maximum ΔS value was acquired when the reaction time was 5 min and this value used for further experiments (ESM Fig. S4B). Finally, the concentration of AgNPs was evaluated for determination of target analyte using the paper-based sensor. For this, 50 μL of 0.1 mM, 0.3 mM, 0.5 mM, and 1 mM AgNPs solution was deposited on the paper substrate and dried at room temperature. Better ΔS values were observed when the concentration of AgNPs was 1 mM AgNPs and this value was further exploited for determination of target analyte from sample solution.

Mechanism for selective determination of Fe^{3+} using smartphone–paper-based sensor impregnated with AgNPs/CTAB

The principle of the sensing mechanism for determination of Fe^{3+} is based on discoloration of CTAB-capped AgNPs which impregnated the paper substrate. The color of AgNPs/CTAB is yellow and addition of analyte on the paper substrate resulted in the discoloration of NPs. The discoloration of AgNPs is due the to aggregation of particles after the addition of analyte on the paper substrate. The preliminary investigation was done by measuring the LSPR absorption band of aqueous solution of CTAB-capped AgNPs in UV–Vis spectrophotometry. The results are shown in ESM Fig. S5. The LSPR

absorption band of AgNPs was found at around 400 nm before the addition of analyte (ESM Fig. S5a), illustrating that the size of the AgNPs was in the range of 10–50 nm [31, 32]. However, broadening and quenching of the absorption band were observed after the addition of analyte into the AgNPs/CTAB as a result of the aggregation of particles (ESM Fig. S5b). Introduction of the analyte into the NP solution caused the aggregation of particles followed by the hypochromic shifts of the absorption peak. There are several reports showing the decrease in absorption of the LPSR band in the visible region after addition of analyte in colorimetric determination of a variety of analytes from different types of samples [23, 24, 28, 29]. The size and shape of NPs were confirmed with TEM before and after the addition of Fe^{3+} into the AgNPs/CTAB solution. Good dispersion of AgNPs could be observed before the addition of analyte (ESM Fig. S5c) and aggregation of particles was observed when NPs were mixed with analyte (ESM Fig. S5d). The lattice structure of of AgNPs is given in ESM Fig. S5e.

Further, the IR spectra of pure CTAB, AgNPs/CTAB, pure iron solution, and mixture of AgNPs/CTAB with iron were recorded in the range of 4000–650 cm^{-1} using FTIR. The results are shown in ESM Fig. S6a–d. The intense peaks observed at 2924 cm^{-1} and 2850 cm^{-1} corresponded to asymmetric and symmetric stretching of CH$_2$ groups of the aliphatic carbon chain of CTAB. The symmetric stretching vibration of the ammonium group (CH$_3$–N$^+$) appeared at 1408 cm^{-1} and asymmetric stretching vibration of CH$_3$–N$^+$ appeared at 1485 cm^{-1} and 1645 cm^{-1} in the spectrum [43] (ESM Fig. S6a, b). The decrease and shift of bands at 1408 cm^{-1} and 1485 cm^{-1} for CH$_3$–N$^+$ demonstrated the interaction of CTAB with AgNPs. This is due to the attachment CH$_3$–N$^+$ of CTAB molecules to the surface of NPs through the physical adsorption forces. ESM Fig. S6c shows the FTIR spectra of ferric iron solution; the bands at 1211 cm^{-1}, 1005 cm^{-1}, and 880 cm^{-1} are assigned to asymmetric and symmetric stretching of sulfate groups (SO$_4^{2-}$) from the standard Fe^{3+} solution prepared from ferric ammonium sulfate [44]. ESM

Fig. S6d shows the IR spectra of AgNPs/CTAB with Fe^{3+} solution; most of the signals are shifted and absorption bands decrease after the addition of analyte into the NP solution because the removal of CTAB molecules from the surface NPs results in the aggregation of AgNPs. Thus, the data obtained from FTIR analysis illustrated the surface modification of NPs with CTAB; and the introduction of analyte perturbing the stability of NPs followed by the color change and hypochromic shift of absorption peak. This phenomenon is further used for determination of Fe^{3+} from sample solution using the smartphone–paper-based sensor.

The aggregation of AgNPs is attributed to the electron transfer reaction taking place on the surface of the AgNPs in the presence of CTAB. Here, the function of CTAB is to stabilize the surface of AgNPs and prevent it from agglomeration. However, the addition of Fe^{3+} into NPs caused the catalytic etching of CTAB from the surface of NPs under acidic conditions which further perturbed the stability of NPs and was followed by aggregation and discoloration of AgNPs. Actually the addition of Fe^{3+} into NPs results in the conversion of Fe^{3+} to Fe^{2+} through the electron transfer reaction from the surface of NPs in the presence of CTAB under acidic conditions. Ganesharajah and Koneswaran also demonstrated the determination of ferric ions from water samples through the electron transfer reaction on the surface of NPs [42] where the reduction of ferric to ferrous ions is demonstrated. In the present work, the conversion of Fe^{3+} to Fe^{2+} through the electron transfer reaction on the surface of NPs is verified by performing different sets of experiments. For this, AgNPs/CTAB was deposited on three test zones of the paper substrate (ESM Fig. S7a–c) and dried at room temperature. The paper substrate containing AgNPs/CTAB and Fe^{3+} exhibited the discoloration because of etching of CTAB from the surface of NPs as well the reduction of Fe^{3+} to Fe^{2+} through the electron transfer reaction (ESM Fig. S7b). This is further confirmed by the addition of 1,10-phenanothroline onto the paper substrate containing converted Fe^{2+} ions (ESM Fig. S7c). The formation of a red-colored Fe(II) complex $[Fe(phen)_3]^{2+}$ on the paper substrate confirmed the formation of ferrous ion after gaining an electron from the NP surface. This discoloration was also observed when ferric irons were added into the CTAB-capped AgNPs. Hence, the sensing mechanism for determination of iron is based on electron transfer reaction using AgNPs/CTAB as a sensing probe under the applied conditions.

Analytical evaluation for determination of total iron using smartphone–paper-based sensor

Analytical validation is a very important part of any newly developed method for determination of a target chemical substance from a sample matrix. Thus, linearity range, limit of detection (LOD), limit of quantitation (LOQ), precision,

accuracy, and selectivity for determination of Fe^{3+} were investigated. The linearity range for determination of substance was determined by drawing the calibration curve by spiking different concentrations of analyte from 50 to 900 μg L^{-1} on the paper substrate impregnated with silver NPs and color intensity was measured using ImageJ software. The color intensity of NPs decreases with increasing concentration of analyte because the discoloration is dependent on the concentration of the analyte on the substrate (Fig. 4A). The linear least-squares equation ($y = mx + c$) was constructed by plotting the ΔS value of signal intensity on the y-axis versus the concentration of analyte on the x-axis (Fig. 4B). A good linear range (50–900 μg L^{-1}) with correlation coefficient of 0.995 (r^2) was acquired for determination of Fe^{3+} using the smartphone–paper-based sensor. The linear least-squares equation ($y = 0.7674x + 97.526$) obtained was used to determine the total iron present in unknown samples. The LOD was calculated by spiking the lowest concentration of analyte on the paper substrate and calculating the standard deviation ($n = 6$). Three times the standard deviation gives the LOD value when the lowest concentration of analyte is deposited on the paper substrate and gives a change in the color intensity of the paper substrate. The LOD value calculated for determination of iron using the smartphone–paper-based sensor was 20 μg L^{-1}. Similarly, LOQ was calculated as ten times the standard deviation when the lowest concentration of analyte was deposited on the paper substrate and gave a change in the signal intensity. The LOQ value for determination of iron using the paper-based sensor was 65 μg L^{-1}. Thus, the linear range, LOD, and LOQ values of the method were estimated for determination of iron in water samples.

Intra-day and inter-day precision of the method is determined by calculating the coefficient of variation (CV) of signal intensity at different concentrations of Fe^{3+} (20, 50,

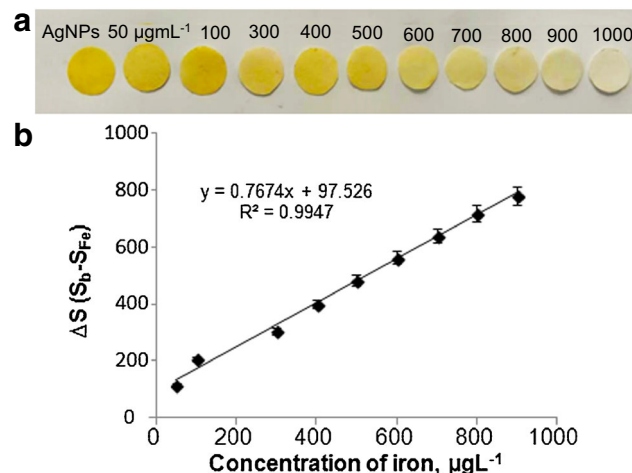Fig. 4 **A** Test zones of filter paper deposited with AgNPs (1 mM) and different concentrations of iron (50, 100, 300, 400, 500, 600, 700, 800, and 900 μg L^{-1}). **B** Calibration curve plotting signal intensity of color developed by ImageJ software versus concentration of ferric iron

100 μg L^{-1}). Intra-day precision is determined by analyzing the particular concentration of analyte at six times in the same day; the inter-day precision is estimated for the same concentration of analyte on six consecutive days. ESM Table S1 shows the value of CV for intra-day and inter-day precision for determination of ferric iron. The better intra-day and inter-day precision values obtained with the present method showed the utility of the smartphone–paper-based sensor for determination of Fe^{3+} from samples.

Accuracy and selectivity of the paper-based sensor were determined by calculating the percentage recovery after the deposition of two different concentrations of Fe^{3+} (100 and 200 μg L^{-1}) on the paper substrate. The relative percentage recovery was calculated by the ratio of concentration of analyte found (calculated using linear least-squares equation) to the amount of analyte added on the paper substrate. Here, the difference in ΔS value was also considered for determination of analyte concentration. The results are given in ESM Table S2. The relative percentage recovery in the range of 91.3–95.0% showed the better accuracy of the proposed method for determination of Fe^{3+} from complex samples. In addition, the good percentage recovery demonstrated the selectivity of the smartphone–paper-based sensor for determination of ferric iron from complex sample matrixes.

Effect of interferents on selective determination of Fe^{3+} using smartphone–paper-based sensor

The selectivity of the smartphone–paper-based sensor impregnated with AgNPs/CTAB was also tested by depositing different metal ions and anions on the paper substrate until the color intensity of NPs changed, a point that was considered the tolerance limit. Thus, metal ions and anions of different concentrations were deposited on the paper substrate and no color change was observed for their given tolerance limit: Na^+, Mg^{2+}, Ba^{2+}, Ca^{2+}, Hg^{2+}, NO_3^- (600 mg L^{-1}); Zn^{2+}, Al^{3+}, Mn^{2+}, As^{3+}, Ni^{2+}, Co^{2+}, CO_3^-, SO_4^{2-} (700 mg L^{-1}); Pb^{2+}, Cu^{2+}, Cd^{2+}, and K^+, Cr^{6+}, Cl^- (800 mg L^{-1}); and PO_4^{3-}

(400 mg L^{-1}). The experimental results demonstrated that the presence of these diverse chemical substances in complex sample matrixes did not affect the determination of Fe^{3+}, illustrating the selectivity of the smartphone–paper-based sensor.

Application of smartphone–paper-based sensor for determination of iron in environmental water and blood plasma samples

The validity of the method was tested by determining the total iron in terms of Fe^{3+} in water and blood plasma samples using the paper-based sensor under the optimized conditions. The filtered water or pretreated water/blood plasma samples (50 μL) were deposited on the paper substrate followed by the addition of $KMnO_4$ and change in color intensity of paper after the deposition of analyte was recorded using ImageJ software. The difference in ΔS ($S_b - S_{Fe}$) value was estimated and the linear least-squares equation was used to determine the concentration of iron present in water/blood plasma samples. Table 1 presents the concentration of iron present in river, pond, tube well water and blood plasma samples. Therefore, the smartphone–paper-based sensor was successfully demonstrated for determination of iron in environmental and biological samples.

Comparison of smartphone–paper-based sensor for determination of iron with other reported methods

The potential of the smartphone–paper-based sensor for determination of iron is compared in terms of linearity range and LOD with other NP-based colorimetric methods such as AuNRs/CTAB [41], AgNPs/citrate [42], AgNPs/agar [45], AuNPs/salicylic acid [3], AuNPs-CTAB + H_2O_2 [7], and MgO NPs [2] (Table 2). A better LOD value for determination of iron is obtained with the present method compared to most of the reported methods except AuNPs–salicylic acid [3] and AuNPs-CTAB + H_2O_2 [7]. The advantages of present work

Table 1 Application of smartphone–paper-based sensor to determination of iron in water and blood plasma samples

Samples/places	AgNPs/CTAB Iron (μg L^{-1})	CV (%) $n = 3$	ICP-AES Iron (μg L^{-1})	CV (%) $n = 3$
River 1/Raipur	137	3.2	129	4.0
River 2/Durg	250	2.8	242	3.1
Pond 1/Raipur	205	2.1	200	3.5
Pond 2/Durg	177	3.0	165	4.1
Tube well 1/Raipur	68	2.6	74	2.5
Tube well 2/Durg	300	3.3	293	3.5
Tube well 3/Dhamtari	105	2.7	109	3.0
Industrial waste water/Raipur	450	3.5	458	2.8
Blood plasma 1	530	2.5	524	3.4
Blood plasma 2	470	3.4	466	4.1

Table 2 Comparison of the paper based sensor for determination of iron with other NPs-based colorimetric methods

Methods	Iron (μM)		Samples	Ref.
	Linearity range	LOD		
AuNRs/CTAB–colorimetry	1.7–178.0	1.7	Water	[40]
AgNPs/citrate–colorimetry	400–1000	130	Water	[41]
AgNPs/agar–colorimetry	0–90	0.54	Water	[42]
AuNPs–salicylic acid–colorimetry	0.3–2.1	0.051	River	[3]
AuNPs-CTAB + H_2O_2–colorimetry	0.20–30	0.067	Blood	[7]
MgO NPs–colorimetry	0–500	23	Water	[2]
PADs-AgNPs/CTAB–smartphone	1.7–16	0.35	Water, blood	Present method

are also compared with those in the work by Ratnarathorn et al. [35] and Apilux et al. [36], who reported paper-based devices for determination of copper and mercury, respectively, using AgNPs as a sensing probe. Here, the sensitivity for determination of mercury using PADs is shown to be low but lack in demonstrating the precision, accuracy, and matrix effects for determination of the target analyte from samples. However, all the methods utilize colorimetry which is expensive compared to our smartphone–paper-based sensor. Here, the smartphone is used for determination of iron and is found to be economic, portable, and can be applied at the sample source.

Further, F test and Student t test were performed to determine the statistical significance difference in the results obtained with paper-based sensor and ICP-AES methods [46]. The formula used for calculation of F test and Student t test is given in ESM. For this, one river water (water 1) and one blood plasma sample (plasma 1) were selected and analyzed using the paper-based sensor and ICP-AES, respectively. The results are given in ESM Tables S3 and S4. The calculated F values for water (1.55) and blood plasma (1.49) samples were lower than the tabulated value (6.26) when the degree of freedom $\upsilon_1 = 5$ and $\upsilon_2 = 4$ at the 95% confidence level. In addition, the values of Student t test ($\pm t$) for water (1.29) and blood plasma (0.93) were lower than the calculated t test (2.262). Since the calculated F and $\pm t$ values were less than their respective tabulated values, there is no significant difference in the results of paper sensor and ICP-AES for determination of iron.

Conclusions

A smartphone–paper-based sensor was successfully demonstrated for determination of total iron in water (river, tube well, pond) and blood plasma samples. The routine analysis of iron is done with sophisticated instruments like AAS, XRF, ICP-AES, ICP-MS, and spectrophotometry which are generally large in size, need trained personnel, require large amounts

of chemical substances, and need time-consuming sample preparation processes. However, the smartphone is portable, user-friendly, economic, and can be applied at the sample source for determination of iron in environmental and biological samples. A development of our paper-based chemical sensor coupled with a smartphone will be miniaturization of the instrument as well as lightweight, cost-effective, flexible, durable devices and can be applied at the sample source. In the near future, smartphone–paper-based chemical sensors can be highly useful for determination of iron in environmental, vegetable, and biological samples.

Compliance with ethical standards

Conflict of interest The authors declare that they have no competing interests.

References

1. Rouault TA. The role of iron regulatory proteins in mammalian iron homeostasis and disease. Nat Chem Biol. 2006;2:406–14.
2. Jain A, Wadhawan S, Kumar V, Mehta SK. Colorimetric sensing of Fe^{3+} ions in aqueous solution using magnesium oxide nanoparticles synthesized using green approach. Chem Phys Lett. 2018;706:53–61.
3. Memon SS, Nafady A, Solangi AR, Al-Enizi AM, Sirajuddin, Shah MR, et al. Sensitive and selective aggregation based colorimetric sensing of Fe^{3+} via interaction with acetyl salicylic acid derived gold nanoparticles. Sensors Actuators B Chem. 2018;259:1006–2012.
4. Dara SS. A textbook of environmental chemistry and pollution control. New Delhi: Chand; 1993.
5. Sahin CA, Tokgoz I, Bektas S. Preconcentration and determination of iron and copper in spice samples by cloud point extraction and flow injection flame atomic absorption spectrometry. J Hazard Mater. 2010;181:359–65.
6. Ke Y, Ming QZ. Iron misregulation in the brain: a primary cause of neurodegenerative disorders. Lancet Neurol. 2003;2:246–53.
7. Liu JM, Wang XX, Jiao L, Cui ML, Lin LP, Zhang LH, et al. Ultra-sensitive non-aggregation colorimetric sensor for determination of

iron based on the signal amplification effect of Fe^{3+} catalyzing H_2O_2 oxidize gold nanorods. Talanta. 2013;116:199–204.

8. Woods J, Mellon M. Thiocyanate method for iron: A spectrophotometric study. Ind Eng Chem Anal Ed. 1941;13:551–4.

9. Hovinen J, Lahti M, Vilpo J. Spectrophotometric determination of thiocyanate in human saliva. J Chem Educ. 1999;76:1281–2.

10. Kass M, Ivaska A. Spectrophotometric determination of iron(III) and total iron by sequential injection analysis technique. Talanta. 2002;58:1131–7.

11. Węgiel K, Robak J, Bas B. Voltammetric determination of iron with catalytic system at a bismuth bulk annular band electrode electrochemically activated. RSC Adv. 2017;7:22027–33.

12. Caprara S, Laglera LM, Monticelli D. Ultrasensitive and fast voltammetric determination of iron in seawater by atmospheric oxygen catalysis in 500 μL samples. Anal Chem. 2015;87:6357–63.

13. Shrivas K, Dewangan K. Surfactant-assisted dispersive liquid–liquid microextraction for sensitive spectrophotometric determination of iron in food and water samples and comparison with atomic absorption spectrometry. J Surfactant Deterg. 2015;18:1137–44.

14. Jorhem L. Determination of metals in foods by atomic absorption spectrometry after dry ashing: NMKL1 collaborative study. J AOAC Inter. 2000;83:1204–11.

15. Bok-Badura J, Jakobik-Kolon A, Turek M, Boncel S, Karonc KA. A versatile method for direct determination of iron content in multi-wall carbon nanotubes by inductively coupled plasma atomic emission spectrometry with slurry sample introduction. RSC Adv. 2015;5:101634–40.

16. Nielson KK, Mahoney AW, Rogers VC. X-ray fluorescence and atomic absorption spectrophotometry measurements of manganese, iron, copper, and zinc in selected foods. J Agric Food Chem. 1988;36:1211–6.

17. Kumar TNK, Revanasidappa HD. Rapid and sensitive spectrophotometric determination of trace amounts of iron(III) using leuco xylene cyanol FF. Anal Bioanal Chem. 2003;376:1126–32.

18. Stalikas CD, Pappas AC, Karayannis MI, Veltsistas PG. Simple and selective spectrophotometric method for the determination of iron(III) and total iron content, based on the reaction of Fe(III) with 1,2-dihydroxy-3,4-diketocyclo-butene (squaric acid). Microchim Acta. 2003;142:43–6.

19. Ahmed MJ, Roy UK. A simple spectrophotometric method for the determination of iron(II) aqueous solutions. Turk J Chem. 2009;33:09–726.

20. Motl NE, Smith AF, DeSantisa CJ, Skrabalak SE. Engineering plasmonic metal colloids through composition and structural design. Chem Soc Rev. 2014;43:3823–34.

21. Zhang JS, Noguez C. Plasmonic optical properties and applications of metal nanostructures. Plasmonics. 2008;3:127–50.

22. Qin L, Zeng Z, Zeng G, Lai C, Duan A, Xiao R, et al. Cooperative catalytic performance of bimetallic Ni-Au nanocatalyst for highly efficient hydrogenation of nitroaromatics and corresponding mechanism insight. Appl Catal B Environ. 2019;259:118035.

23. Fu Y, Qin L, Huang D, Zeng G, Lai C, Li B, et al. Chitosan functionalized activated coke for Au nanoparticles anchoring: green synthesis and catalytic activities in hydrogenation of nitrophenols and azo dyes. Appl Catal B Environ. 2019;255:117740.

24. Shrivas K, Shankar R, Dewangan K. Gold nanoparticles as a localized surface plasmon resonance based chemical sensor for on-site colorimetric determination of arsenic in water samples. Sensors Actuators B Chem. 2015;220:1376–83.

25. Shrivas K, Nirmalkar N, Ghosale A, Thakur SS, Shankar R. Enhancement of plasmonic resonance through an exchange reaction on the surface of silver nanoparticles: application to the highly selective determination of triazophos pesticide in food and vegetable samples. RSC Adv. 2016;6:80739–47.

26. Rohita JV, Solankib JN, Kailasa SK. Surface modification of silver nanoparticles with dopamine dithiocarbamate for selective colorimetric sensing of mancozeb in environmental samples. Sensors Actuators B Chem. 2014;200:219–26.

27. Shrivas K, Sahu S, Sahu B, Kurrey R, Patle TK, Kant T, et al. Silver nanoparticles for selective detection of phosphorus pesticide containing π-conjugated pyrimidine nitrogen and sulfur moieties through non-covalent interactions. J Mol Liq. 2019;275:297–303.

28. Khalililaghab S, Momeni S, Farrokhnia M, Nabipour I, Karimi S. Development of a new colorimetric assay for detection of bisphenol-A in aqueous media using green synthesized silver chloride nanoparticles: experimental and theoretical study. Anal Bioanal Chem. 2017;409:2847–58.

29. Shrivas K, Sahu S, Ghorai A, Shankar R. Gold nanoparticles-based colorimetric determination of cationic surfactants in environmental water samples via both electrostatic and hydrophobic interactions. Microchim Acta. 2016;183:827–36.

30. Qin L, Zeng G, Lai C, Huang D, Zhang C, Xu P, et al. A visual application of gold nanoparticles: simple, reliable and sensitive detection of kanamycin based on hydrogen-bonding recognition. Sens Actuators B. 2017;243:946–54.

31. Laliwala SK, Mehta VN, Rohit JV, Kailasa SK. Citrate-modified silver nanoparticles as a colorimetric probe for simultaneous determination of four triptan-family drugs. Sensors Actuators B Chem. 2014;197:254–63.

32. Shrivas K, Nirmalkar N, Thakur SS, Kurrey R, Sinha D, Shankar R. Experimental and theoretical approaches for the selective detection of thymine in real samples using gold nanoparticles as a biochemical sensor. RSC Adv. 2018;8:24328–37.

33. Zhang XX, Song YZ, Fang F, Wu ZY. Sensitive paper-based analytical device for fast colorimetric detection of nitrite with smartphone. Anal Bional Chem. 2018;410:2665–9.

34. Nery EW, Kubota LT. Sensing approaches on paper-based devices: a review. Anal Bioanal Chem. 2013;405:7573–95.

35. Ratnarathorn N, Chailapakul O, Henry CS, Dungchai W. Simple silver nanoparticle colorimetric sensing for copper by paper-based devices. Talanta. 2012;99:552–7.

36. Apilux A, Siangproh W, Praphairaksit N, Chailapakul O. Simple and rapid colorimetric determination of Hg(II) by a paper-based device using silver nanoplates. Talanta. 2012;97:388–94.

37. Chen Y, Fu G, Zilberman Y, Ruan W, Ameri SK, Zhang YS, et al. Low cost smart phone diagnostics for food using paper-based colorimetric sensor arrays. Food Control. 2017;82:227–32.

38. Patel KS, Shrivas K, Brandt R, Jakubowski N, Corns W, Hoffmann P. Arsenic contamination in water, soil, sediment and rice of central India. Environ Geochem Health. 2005;27:131–45.

39. Kingsle GR, Getchell G. Serum iron determination. Clin Chem. 1956;2:175–83.

40. Shrivas K, Wu HF. Applications of silver nanoparticles capped with different functional groups as the matrix and affinity probes in surface-assisted laser desorption/ionization time-of-flight and atmospheric pressure matrix-assisted laser desorption/ionization ion trap mass spectrometry for rapid analysis of sulfur drugs and biothiols in human urine. Rapid Commun Mass Spectrom. 2008;22:2863–72.

41. Thatai S, Khurana P, Prasad S, Kumar D. A new way in nanosensors: gold nanorods for sensing of Fe(III) ions in aqueous media. Microchem J. 2014;113:77–82.

42. Ganesharajah M, Koneswaran M. Citrate capped silver nanoparticles as optical sensor for ferric ions. Int J Nano Med Eng. 2018;3:63–70.

43. Jiang Z, Xie J, Jiang D, Wei X, Chen M. Modifiers-assisted formation of nickel nanoparticles and their catalytic application to p-nitrophenol reduction. CrystEngComm. 2013;15:560–9.

44. Frosta RL, Xi Y, Scholz R, Lopez A, Granja A. Infrared and Raman spectroscopic characterisation of the sulphate mineral creedite—$Ca_3Al_2SO_4(F,OH)\cdot2H_2O$—and in comparison with the alums. Spectrochim Acta Part A. 2013;109:201–5.

45. Basiria S, Mehdinia A, Jabbari A. A sensitive triple colorimetric sensor based on plasmonic response quenching of green synthesized silver nanoparticles for determination of Fe^{2+}, hydrogen peroxide, and glucose. Colloids Surf A Physicochem Eng Asp. 2018;545:138–46.

46. Christian GD. Analytical chemistry, 6th edn. New Delhi: Wiley India; 2007. p. 1–856.